Multimode solitons in step-index fibers

Mario Zitelli, Yifan Sun, Mario Ferraro, Fabio Mangini, Oleg Sidelnikov, Vincent Couderc, Stefan Wabnitz

Multimode solitons in step-index fibers

MARIO ZITELLI,[1,*] YIFAN SUN,[1] MARIO FERRARO,[1] FABIO MANGINI,[2] OLEG SIDELNIKOV,[3] VINCENT COUDERC,[4] AND STEFAN WABNITZ[1,3]

[1] *Department of Information Engineering, Electronics and Telecommunications, Sapienza University of Rome, Via Eudossiana 18, 00184 Rome, Italy*
[2] *Department of Information Engineering, University of Brescia, Via Branze 38, 25123 Brescia, Italy*
[3] *Novosibirsk State University, Pirogova 1, Novosibirsk 630090, Russia*
[4] *Université de Limoges, XLIM, UMR CNRS 7252, 123 Avenue A. Thomas, 87060 Limoges, France*
[*] *mario.zitelli@uniroma1.it*

Abstract: We experimentally generate multimode solitons in step-index fibers, where nonlinearity compensates for both chromatic and modal dispersion. These solitons are subject to Raman self-frequency shift, and their energy is gradually transfered to the fundamental fiber mode. We compare multimode soliton dynamics in both step-index and graded index fibers, in excellent agreement with numerical predictions.

1. Introduction

In recent years, there has been a growing research interest in the study of optical pulse propagation in nonlinear multimode fibers. This has been motivated from several emerging technological applications, such as enhancing the information capacity of optical communication links [1], or scaling up the energy delivered by fiber lasers [2]. In this context, the possibility of generating multimode optical solitons was theoretically proposed in 1980 by Hasegawa [3]. Early experiments by Grudinin et al. demonstrated soliton generation in graded index fibers (GIFs). Remarkably, a highly multimode laser pump at 1064 nm could generate, via cascaded stimulated Raman scattering, femtosecond pulses undergoing Raman soliton self-frequency shift (SSFS), with a beam waist close to that the fundamental mode [4].

Systematic experimental studies of the properties of multimode optical solitons, or spatiotemporal solitons, have only been carried out in the past few years [5–9]. So far, all of these studies involved the use of GIFs, which are particularly suited for nonlinear optics because of their relatively low modal dispersion, as well as the strong four-wave mixing interactions that are allowed by multiple phase-matching conditions for the modes with equally spaced propagation constants. Although all of these experiments have reported that Raman solitons in GIFs tend to emerge in the fundamental mode of the fiber, the multimode nature of the soliton generation mechanism was not confirmed until very recently. Experiments have shown that the conditions leading to soliton generation in GIFs are based on the mechanism of balancing, via the Kerr nonlinearity, both intramodal (or chromatic) and intermodal dispersion [10]. On the other hand, by injecting ultrashort pulses in appropriate higher-order modes (HOMs) of step-index fibers (SIFs), frequency-shifted solitons in different HOMs were generated from noise via Raman scattering, by compensating chromatic dispersion walk-off with modal dispersion [11]. To our knowledge, the generation of multimode solitons in SIFs has not been reported yet. Specifically, no systematic experimental or even theoretical study about the modal content of SIF solitons was ever carried out.

In this work, we experimentally demonstrate the spatial beam cleanup of femtosecond Raman solitons in SIFs, for different input beam coupling conditions. Moreover, we carry out a detailed intercomparison of soliton beam cleaning in SIFs and in GIFs. In GIFs, a multimode walk-off

soliton is initially formed, which only includes non-degenerate axial modes [10]. Whereas in SIFs the generated Raman multimode soliton is initially composed by the LP_{01}, LP_{11a} and LP_{11b} modes only: remaining HOMs are confined at the input pump wavelength. Similar to the case of GIFs, we observed that also in SIFs the long-term evolution of the Raman multimode soliton results into a fundamental mode soliton. Numerical simulations fully support the experimental results. Finally, we propose a theoretical interpretation of the observed soliton pulsewidth, by showing that the mechanism of balancing chromatic and modal dispersion with nonlinearity, which underlies the formation of walk-off solitons [10], also describes multimode soliton generation in SIFs.

2. Experimental evidence

In our experimental setup, we used an optical parametric amplifier (OPA) to generate 70 fs pulses at 1450 nm with 100 kHz repetition rate. These pulses were injected into multimode fibers (MMFs) with a Gaussian beam shape, and $1/e^2$ input diameter of approximately 30 μm (15 μm beam waist, $M^2 = 1.3$). We used two, 10 m long spans of SIF and GIF, respectively. The GIF had a core radius $r_c = 25$ μm, cladding radius 62.5 μm, cladding index $n_{\text{clad}} = 1.445$ at 1450 nm, and relative index difference $\Delta = 0.0103$. The SIF was a commercial 50/125 μm fiber with numerical aperture $NA = 0.2$ (Thorlabs FG050LGA). The laser pulse input energy was controlled by means of an external attenuator, and varied between 0.1 nJ and 60 nJ. At the fiber output, a micro-lens focused the near field on an InGaAs camera (Hamamatsu C12741-03); a second lens focused the beam into a real-time multiple octave spectrum analyzer (Fastlite Mozza) with a spectral detection range of 1100-5000 nm. The output pulse temporal shape was inspected by an intensity autocorrelator (APE pulseCheck 50) with femtosecond resolution.

We tested two different input coupling regimes into the SIF: axial coupling (on-axis input beams), and non-axial coupling (input beams with 10 μm off-axis coupling). For GIFs, only the axial case was considered, because non-axial coupling did not produce any noteworthy differences. Using field overlap integrals, we calculated the modal power fraction distribution at the fiber input, which is equal to 52%, 30%, 18% for the axial modes LG_{01}, LG_{02}, and LG_{03}, respectively, in the case of a GIF with axial coupling, and to 95%, 0.3%, and 0.6% for modes LP_{01}, LP_{02}, and LP_{03}, respectively, in the case of an SIF with axial coupling; the remaining power being distributed among HOMs. In the case of SIF with non-axial coupling, the calculated input power fraction was 60%, 30%, 4%, 0.4% for modes LP_{01}, LP_{11}, LP_{21}, LP_{31} respectively; the remaining power fraction was distributed among other HOMs. The input power distributions are possibly modified by bending, along pulse propagation in the fiber.

In Fig. 1, we compare the input pulse energy dependence of the experimental output spectra after 10 m of fiber transmission, for three different cases. Specifically: a) SIF with axial coupling; b) SIF with 10 μm offset of the input beam (non-axial coupling); c) GIF with axial coupling. Here the white lines are guides to the eye, and indicate the position of the mostly red-shifted spectral peak. Note that different input energy ranges are used in each of the panels of Fig. 1. In the figure, for each input energy the spectrum is normalized to its peak value, in order to compare the shape of the evolution of the red-shifted spectral lobes.

In all of the three cases, a Raman soliton spectrum separates from a residual pump wave, and it is red-shifted by a wavelength amount that increases nearly quadratically with the input pulse energy. Moreover, the observed Raman soliton spectra at the fiber output fit very well to the hyperbolic secant shape of a soliton. In addition, the output pulsewidth and beam waist of the Raman solitons reduce to a minimum at a given value of the input pulse energy, as it will be shown below. Hence, we may conclude that in all cases a Raman soliton is generated, which experiences SSFS up to 1750 nm as the input pulse energy grows larger. When using a SIF with axial coupling, see Fig. 1(a), for sufficiently high input pulse energies, several spectral lobes are observed at the fiber output. Each lobe corresponds to an individual pulse, which is generated

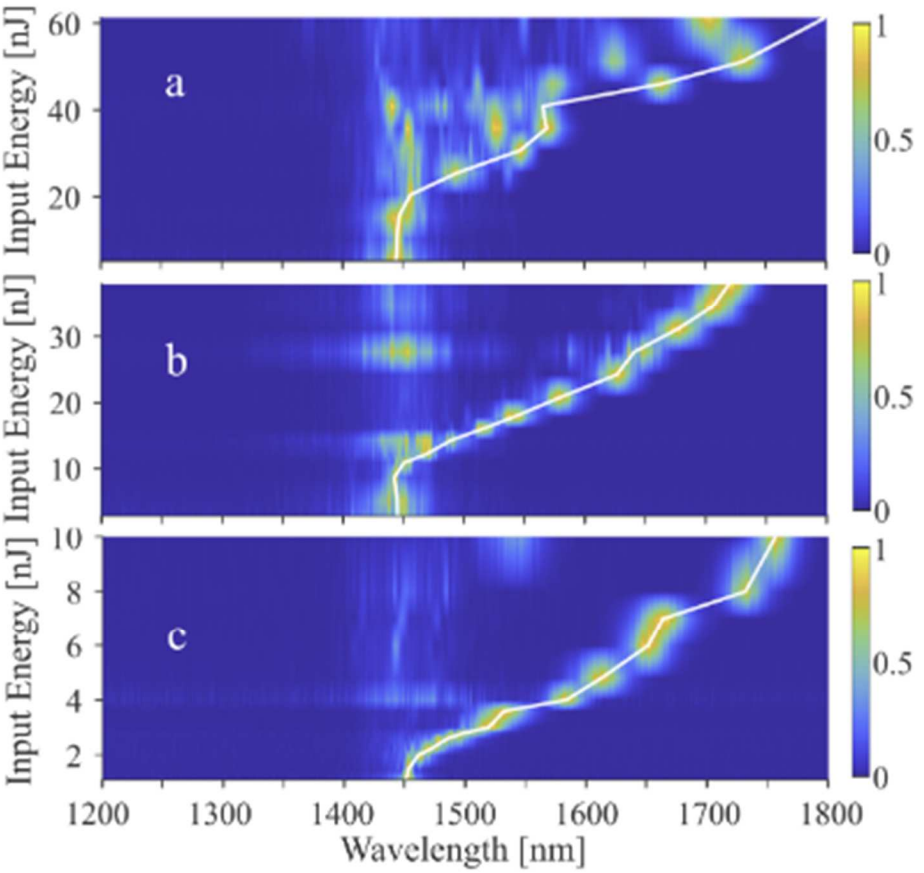

Fig. 1. Output spectra vs. input pulse energy for: a) 10 m of SIF, axial coupling; b) 10 m of SIF with non-axial coupling; c): 10 m of GIF with axial coupling. White lines are guides to the eye, for marking the most red-shifted spectral peak.

from the fission of the input multisoliton pulse. Note that, when a secondary Raman soliton is generated, the energy available for the first Raman soliton emerging from the fission is reduced. As a result, the most red-shifted Raman soliton pulse decreases its rate of frequency shift, and an irregular wavelength shift is observed, as in the case of 35-40 nJ input energy. When non-axial coupling is used, see Fig. 1(b), a single dominant soliton spectrum is formed at 12 nJ input energy; it will be shown later that this results from the generation of a single spatiotemporal soliton, that includes the three lowest-order modes. The spectral lobe of the Raman soliton undergoes a well-defined self-frequency shift starting from 1450 nm, and increasing continuously with the input energy, with no wavelength jump. The presence of residual spectral lobes is not as evident as in the case of Fig. 1(a), with the exception of a secondary large spectral lobe at 1450 nm, which appears for an input pulse energy of 27 nJ; the origin of this secondary large spectrum is the formation of a soliton molecule (or bound state of multiple solitons) after the initial pulse fission; the detailed study of such a molecule goes beyond the scope of this work. In the case of a GIF with axial coupling, see Fig. 1(c)), the Raman soliton is the dominant spectral feature, exhibiting a continuous SSFS. The presence of a residual pump wave is considerably reduced in a GIF, except for input energies above 6 nJ; yet, this wave carries less than 20% of the total input energy.

The appearance of step-wise wavelength changes for the generated Raman soliton, in the case of SIF with axial coupling, is better illustrated in Fig. 2. Here we show, for each of the three cases reported in Fig. 1, the input energy dependence of the wavelength of the most red-shifted spectral lobe. As shown by selected spectra (see insets), in a SIF with axial coupling a spectrum containing multiple lobes (located at either the pump or the soliton wavelength) appears at 25 nJ, after input pulse fission and multimode soliton formation; this follows an initial spectral

narrowing at 20 nJ of input energy [12], as it is illustrated in the fourth inset of the figure. Whereas, in the case of a SIF with non-axial input coupling, solitons undergo a gradual Raman self-frequency shift, and secondary lobes are less visible. Figure 2 shows that, after a spectral narrowing at 9 nJ which is illustrated in the first inset, a single soliton spectrum appears at 12 nJ of input energy; for higher energies, this soliton continuously red-shifts because of self-induced Raman scattering. Multimode soliton formation appears at a lower input pulse energy in a SIF with non-axial coupling, when compared with the axial coupling case, because with non-axial coupling modes LP_{11a} and LP_{11b} possess a larger power fraction at the fiber input. As a result, a multimode soliton including these two modes plus the fundamental LP_{01} mode is generated. In the case of a SIF with axial coupling, the launched axial modes LP_{01}, LP_{02}, LP_{03} require higher input energy for multimode soliton formation, in order to counteract the larger amount of modal dispersion among them, as it will be explained in the remainder of this paper. The spectral narrowing which is observed immediately before the soliton formation is caused by the interplay of the cumulated anomalous dispersion and the self-phase modulation (SPM) which is experienced by the input pulse. Note that, although in this case the pulse peak power is still below the threshold for soliton generation, yet it is sufficient to introduce a significant nonlinear chirp.

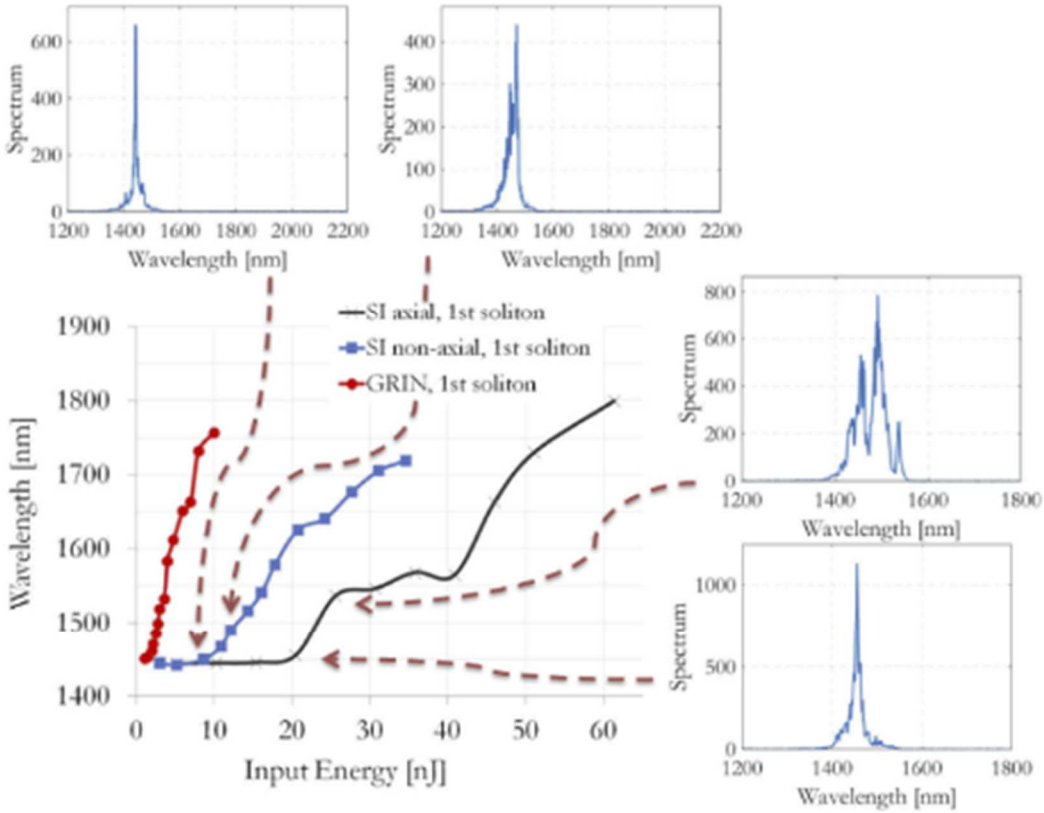

Fig. 2. Wavelength of the most red-shifted spectral lobe vs. input pulse energy for the three cases of Fig. 1. Output spectra are reported for the cases indicated by the arrows.

When considering the near-field of the output beams, Fig. 3 reports three rows corresponding to the cases presented in Fig. 1(a)–1(c), respectively. Here the left column shows the output beams at relatively low pulse energies, below the threshold for generating the Raman soliton. Whereas central and right columns in Fig. 3 illustrate output beams in the nonlinear regime. These are measured at the fiber output after inserting either a 1500 nm short-pass filter or a 1500 nm long-pass filter, respectively. Hence, the central (right) column in Fig. 3 shows output beams of residual pump light at 1450 nm (Raman red-shifted soliton beams). As it can be seen from the top row of Fig. 3 (corresponding to Fig. 1(a)), at high pulse energies the residual pump beam

is clearly dominated by mode LP_{11}, and it appears to lack any significant fundamental mode component. Whereas the Raman soliton beam shape is close to that of the fundamental mode of the SIF: the beam waist is 18.2 μm. The middle row of Fig. 3 (corresponding to Fig. 1(b)) reveals that, for low input pulse energies, a highly multimode pattern is observed, including an LP_{01} mode component. Whereas for high input energies, the residual pump beam is dominated by the LP_{21} and LP_{31} modes, and it lacks the fundamental mode of the SIF (no central beam component). On the other hand, the Raman soliton beam is once again close to the LP_{01} mode of the SIF: here we recorded a minimum beam waist of 16.4 μm. Finally, the bottom row of Fig. 3 (corresponding to Fig. 1(c)), reveals that, for both low and high input pulse energies, the output beam at the input pump wavelength is a superposition of axial modes (i.e., modes LG_{01} and LG_{02}). Whereas the beam of the Raman soliton is mainly carried by the fundamental mode LG_{01} of the GIF, with a measured minimum beam waist of 7.9 μm.

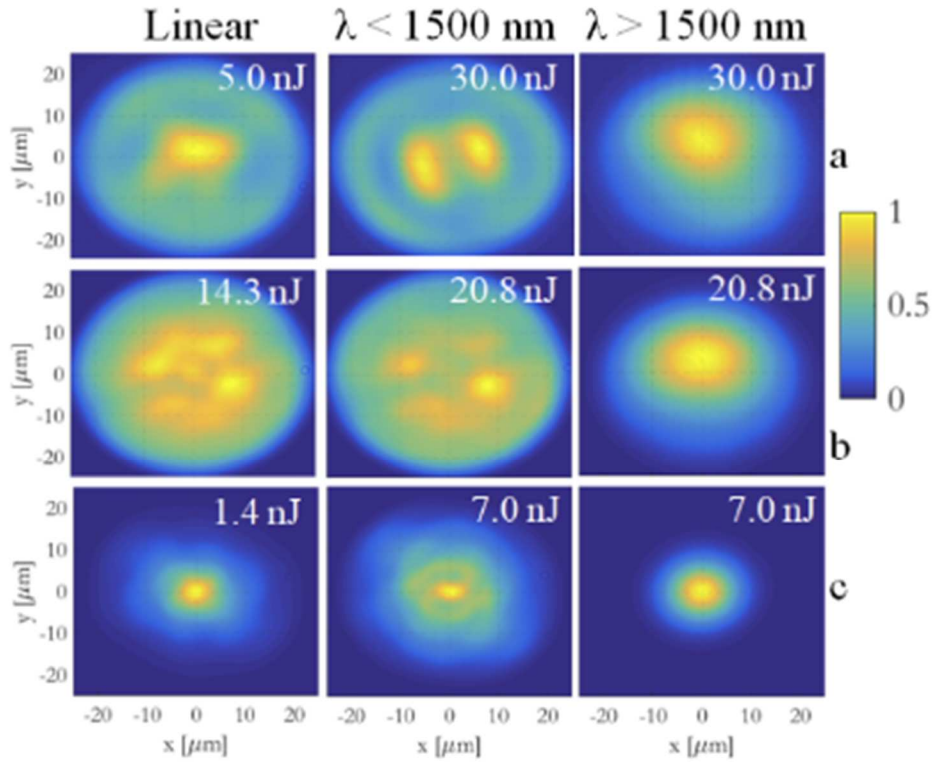

Fig. 3. Output beam from 10 m of fiber length for: SIF with axial coupling (row a); SIF with non-axial coupling (row b); GIF with axial coupling (row c). Left column: linear regime; central and right columns: nonlinear regime with output low-pass and long-pass filters, respectively.

To provide more details of the nonlinear evolution of the Raman soliton beams, in Fig. 4 we illustrate the dependence on input pulse energy of the output beam waist, for each of the three cases that were considered in Fig. 1(a)–1(c). We separately measured the output beam waist of the residual pump beam or of the Raman soliton, by placing either a 1500 nm short-pass or a long-pass filter, respectively. The beam waist was measured at $1/e^2$ radius of the near field, collected by the InGaAs camera, and averaged over the x and y transverse axes. Beam radius was also calculated using the second-moment equations according to the standard ISO11146, and plotted as dashed curves with same colors. Beam waist and radius provide similar curves, being almost identical in correspondence of the beam condensation regime (e.g., around 3 nJ of input energy for GIF, and 16 nJ for SIF with non-axial excitation). In order to perform a direct comparison of the condensed beam with the Gaussian beam theory, we will use the measured waist in the following discussion. Figure 4 shows that, for a SIF with non-axial input beams (not

shown, axial input), and for all input pulse energies, the waist of the residual pump wave remains close to 23 μm, which is similar to the fiber core radius. Whereas the waist of the Raman soliton beam (i.e., for λ>1500 nm) in the non-axial input coupling case is equal to 18.0 μm when the soliton is initially formed, and it reduces down to 16.4 μm at 16 nJ of input pulse energy. For larger input energies, the Raman soliton beam waist grows monotonically up to 20.0 μm. Whereas in the case of axial beam coupling, the initial soliton waist equals 18.9 μm at 25 nJ, and it reduces to 18.1 μm at 35 nJ of input pulse energy. The measurement error from the InGaAs camera was 0.25 μm/pixel; hence, the waist oscillations observed in the Raman beam curves for different input energies are not ascribed to measurement errors, but they arise from small deformations of the output beam. Note that the beam waist of the fundamental mode in the SIF is given by the Marcuse equation for the mode field diameter [13] $\mathrm{MFD}/2 = a(0.65 + 1.619/V^{1.5} + 2.879/V^{6})$, where a is the fiber core radius, and $V = k_0 a\mathrm{NA}$ is the normalized frequency. The fundamental mode waist at 1500 nm is 16.6 μm, which is close to the measured waist minimum of the Raman soliton beams. Overlap integrals were calculated with comparison to a Gaussian beam with 16.6 μm waist; we obtained an overlap fraction of 97% and 84% for the non-axial and axial cases at 21 nJ and 51 nJ input energy, respectively. Gaussian fits were also performed for the horizontal and vertical beam profiles, providing fit R-squared factors of 0.995 and 0.988 in the two cases. These results indicate that with both axial or non-axial input coupling, a Raman soliton carried by the fundamental mode of the SIF is observed. Furthermore, the Raman soliton reaches the narrowest beam waist values as soon as it is generated above 1500 nm: after the short-pass filter, no beam reduction is observed.

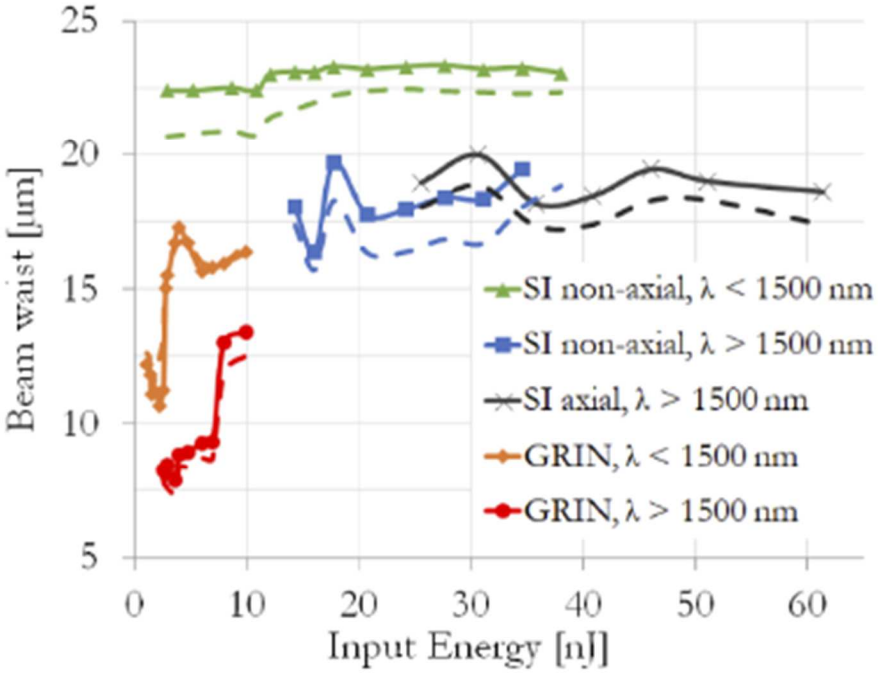

Fig. 4. Output beam waist vs. input energy, for the three cases of Fig. 1, measured after a 1500 nm short-pass or long-pass filter, respectively. Dashed lines provide the beam radius from second-moment equations.

On the other hand, Fig. 4 shows that, when a GIF is used, a nonlinear beam waist reduction is also observed around the pump wavelength (i.e., when measuring the beam from a 1500 nm short-pass filter). Specifically, when the input pulse energy is increased from 1.1 nJ to 2.2 nJ, the output beam waist decreases from 12.2 μm down to 10.6 μm. The beam width is further reduced for the Raman soliton (as it is measured from 1500 nm long-pass filter): a minimum beam waist of 8.0 μm is obtained when the soliton is formed at 2.8 nJ of input pulse energy.

This is consistent with the generation of a spatiotemporal Raman soliton, including HOMs, originating from the fission of the input pump pulse; the soliton is initially formed at the pump wavelength, and subsequently it experiences SSFS [9]. The waist of the fundamental mode in a GIF can be obtained from the beam self-imaging theory, which describes the periodic replication of the field during the propagation. One of the parameters associated with the dynamics of beam propagation in a GIF is the so-called beam oscillation parameter C, which is related to the beam oscillation amplitude [14,15]. Specifically, when C takes the extreme value $C = 1$, the beam amplitude remains constant, thus indicating that only the fundamental mode is excited. Starting from this consideration, one easily obtains for the beam waist $w_e = (\lambda a/\sqrt{2\Delta}\pi n_{\text{eff}})^{0.5}$, where Δ is the relative index difference and n_{eff} the modal index. At the Raman soliton wavelength of 1520 nm, one obtains a fundamental mode waist of 7.6 μm, which is close to the measured minimum value at 2.8 nJ. The overlap integral between the beam at 2.8 nJ input energy, and a Gaussian beam with 7.6 μm waist equals 85%; Gaussian fits for the horizontal and vertical beam profiles provided a R-squared value of 0.999. As a matter of fact, in GIFs we always observed that the output Raman solitons are carried by the fundamental mode, as confirmed by numerical simulations.

The solitonic nature of the observed Stokes pulses corresponding to the cases in Fig. 1(a)–1(c) is confirmed by measuring their output pulsewidth after the 1500 nm long-pass filter (see Fig. 5). In the case of a SIF with non-axial input coupling one obtains a minimum pulse duration of 103 fs at 21 nJ of input pulse energy. In SIF with axial coupling the output pulses exhibit a monotonic decrease of temporal duration when the input energy grows larger, down to 125 fs for 50 nJ input pulses. On the other hand, Fig. 5 shows that in GIFs the output pulse duration sharply decreases from 260 fs down to 90 fs at 2.8 nJ input energy, which is precisely the energy value leading to minimum beam waist. As recently discussed [10], in GIFs this behavior corresponds to the generation of walk-off solitons. In the concluding section it will be shown that the walk-off soliton condition also applies to SIFs.

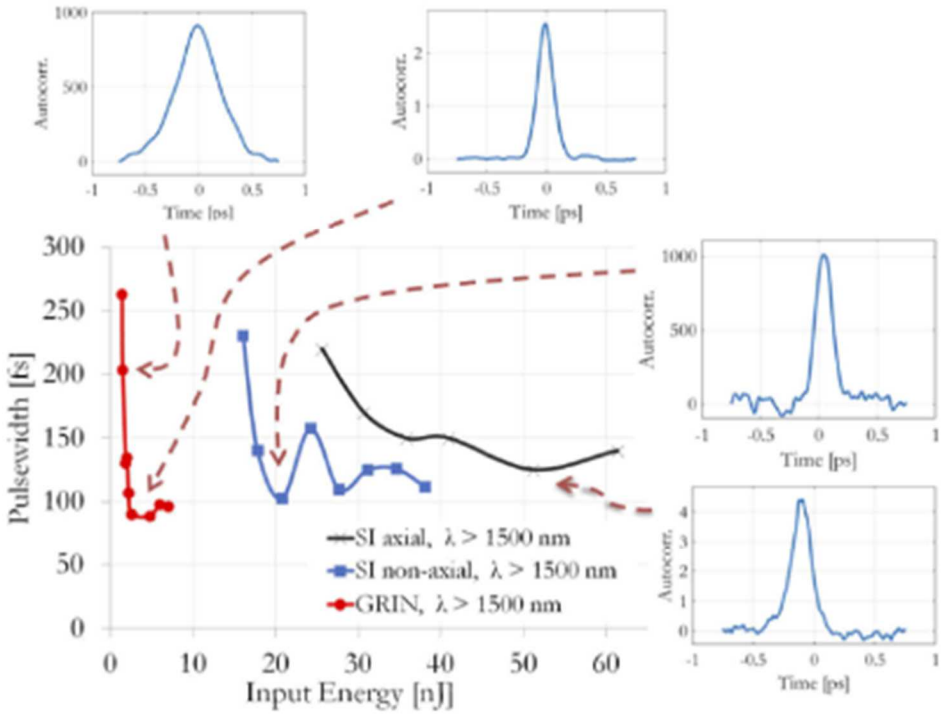

Fig. 5. Output pulsewidth vs. input energy, for the 3 cases of Fig. 1, and after 1500 nm long-pass filter. The insets are autocorrelation traces corresponding to the indicated data points.

In a GIF, the theoretical value for a fundamental mode soliton energy is [16] $E_1 = (\lambda|\beta_2|w_e^2)/n_2T_0$, where β_2 is the fiber dispersion at the soliton wavelength, $T_0 = T_{\mathrm{FWHM}}/1.763$, and $n_2 = 2.7 \times 10^{-20}$ m^2/W is the nonlinear index. One calculates a soliton energy of 2.4 nJ, which is close to the measured value for the Raman soliton, that is generated for 2.8 nJ of input pulse energy. Indeed, output soliton spectrum measurements provide the experimental soliton energy of 2.3 nJ; a residual portion of the input pulse energy remains as a dispersive wave at the initial wavelength.

In the case of a SIF with non-axial input, by using the experimental Raman soliton pulse duration of 103 fs at the 1620 nm output wavelength, and the 16.6 μm beam waist, one estimates a theoretical fundamental soliton energy of 22 nJ; the measured input energy for soliton formation was 21 nJ; according to the calculated modal power fraction, 90% of the input energy (19 nJ) is carried by the modes LP_{01}, LP_{11a}, LP_{11b} which form the multimode soliton: such energy value is fairly close to the theoretical value. This indicates that a Raman soliton is formed in this case as well. On the other hand, as shown in Fig. 5, in the case of a SIF with axial input the soliton generation process is less efficient.

3. Numerical results

Numerical simulations were performed, in order to verify the Raman soliton generation process in both SIFs and GIFs. The model we used is based on solving coupled-mode equations [17,18]. The modal distribution of power at the fiber input was calculated by means of field superposition integrals. The model couples the propagating mode fields through the Kerr nonlinearity, via four-wave mixing (FWM) terms of the type $Q_{plmn}A_lA_mA_n^*$ (where Q_{plmn} are coupling coefficients, proportional to the overlap integrals of transverse modal field distributions), and via stimulated Raman scattering (SRS) terms with the same coupling coefficients. GIF dispersion and nonlinearity parameters were $\beta_2 = -17.1$ ps^2/km for mode LG_{01} at 1450 nm, and $\beta_3 = 0.099$ ps^3/km. The SIF dispersion was $\beta_{2_2} = -17.6$ ps^2/km for mode LP_{01} at 1450 nm, and $\beta_3 = 0.118$ ps^3/km. The nonlinear index n_2 was the same for both fibers, and the Raman response $h_R(t)$ had typical time constants of 12.2 and 32 fs [19,20]. Wavelength-dependent linear losses of silica were included.

In Fig. 6(a) we show the simulated output spectrum after 10 m of SIF, with 24 nJ input pulse energy distributed as follows: 60% is assigned to mode LP_{01}, and 6.6% to each of the modes LP_{11a}, LP_{11b}, LP_{21a}, LP_{21b}, LP_{31a}, LP_{31b}. These coupling conditions provide comparable results with the non-axial coupling case of Figs. 1(b) and 3(b); considerable power was provided to HOMs in order to show that, in any case, the spatiotemporal soliton formation is limited to the first few modes. The generated Raman soliton shifts its wavelength to 1620 nm, and it only includes the LP_{01} mode after 10 m distance, since the fundamental mode has captured all of the energy of modes LP_{11a}, LP_{11b}, as it is illustrated in Fig. 6(c). The residual HOMs remain at the input wavelength of 1450 nm. For a better comparison with experiments, the calculated output beams after either long-pass or short-pass filters at 1500 nm are provided in the insets: a good fit with the experimental results of Fig. 3(b) is obtained. The simulated temporal pulse evolution (not shown), corresponding to the spectra in Fig. 6(a), as well as the modal energy evolution with distance represented in Fig. 6(c), confirm that the mode LP_{01} initially couples with the quasi-degenerate modes LP_{11a}, LP_{11b} to form a multimode soliton. Upon subsequent propagation, the fundamental mode collects the energy of these quasi-degenerate modes: no long-term stable trapping of multiple modes is observed in the SIF.

Figure 6(b) shows, for a comparison, the simulated spectrum from 10 m of GIF with 5 nJ input pulse energy, for the case of axial coupling, including axial modes LG_{01}, LG_{02}, LG_{03}, and with fraction of power 52%, 30%, 18%, respectively. The case corresponds to the experimental data of Fig. 3(c). In a GIF, a multimode walk-off soliton is initially formed, involving the trapping of the fundamental mode with axial HOMs. Also in this case, upon propagation the HOMs gradually

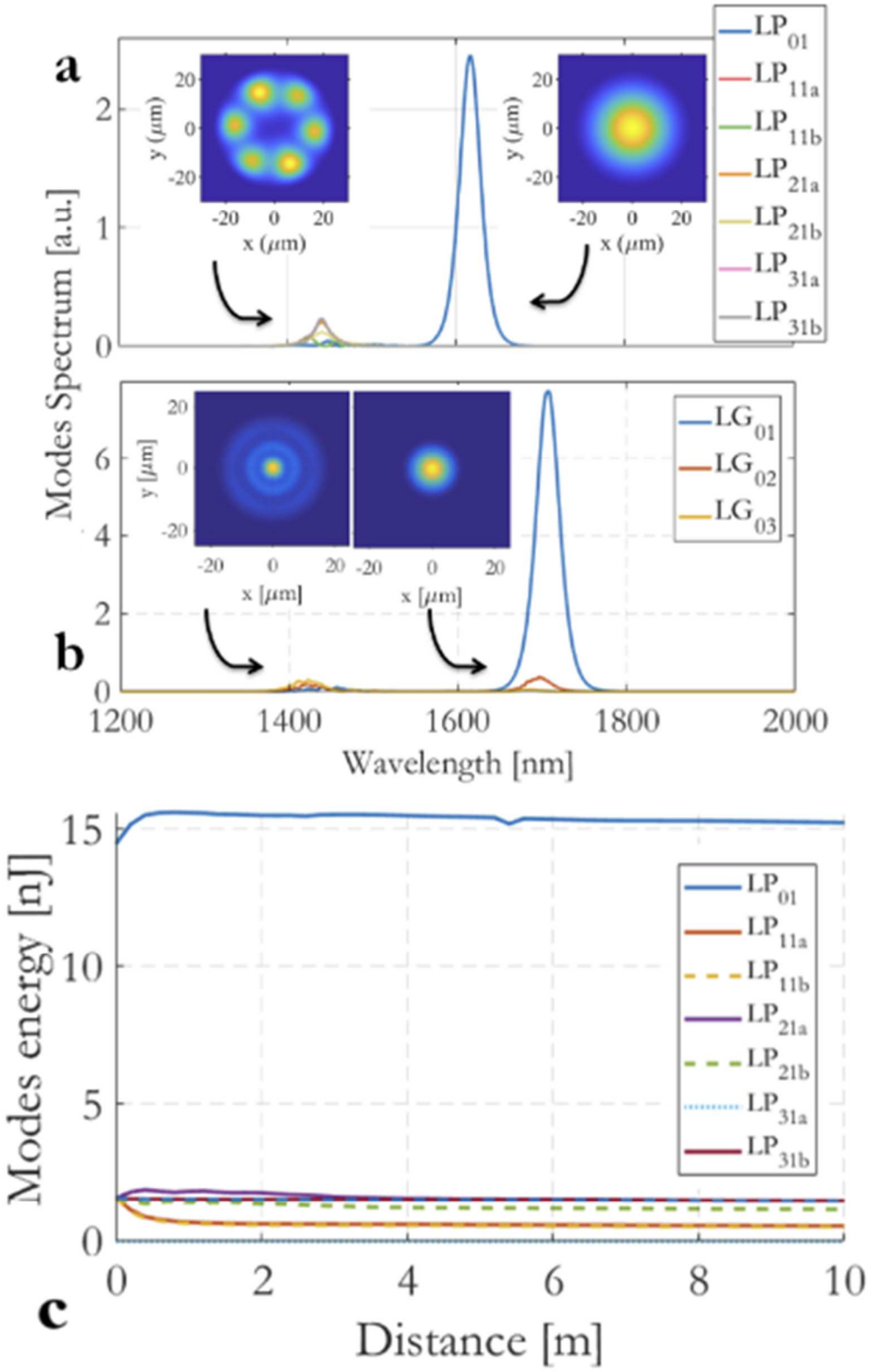

Fig. 6. Simulated output spectra for: a) 10 m of SIF with 24 nJ input pulse energy, including modes LP_{01}, LP_{11a}, LP_{11b}, LP_{21a}, LP_{21b}, LP_{31a}, LP_{31b} with power fractions: 60% for LP_{01} and 6.6% for other modes. b): 10 m of GIF with 5 nJ input pulse energy, including axial modes LG_{01}, LG_{02}, LG_{03}, with power fraction of 52%, 30%, and 18%, respectively. Insets show output beams for the soliton and the residual pump wave, respectively. c): simulated modal energy evolution vs. distance, for the case of Fig. 6(a).

transfer their energy into the fundamental mode [9]. The short-pass filtered beam, which is

shown in the inset of Fig. 6(b), is indeed composed by all input three axial modes. Whereas the long-pass filtered beam is mostly composed by the LG_{01} fundamental mode.

4. Discussion and conclusions

Similarly to the case of GIFs, the multimode soliton generation mechanism in SIFs can also be explained in terms of the walk-off soliton concept [10], whereby nonlinearity compensates for both intramodal and intermodal dispersion. As suggested by numerical simulations and by experimental observations, a spatiotemporal soliton in SIFs is initially composed by the LP_{01}, LP_{11a}, LP_{11b} modes only; according to the theory, a walk-off soliton forms when the chromatic dispersion length L_D, the nonlinearity length L_{NL}, and the modal walk-off length L_W, averaged among the modes composing the soliton, are nearly the same; namely, $L_D = L_{NL} = const \cdot L_W$. The pulsewidth of the soliton immediately after its formation is then given by $T_{\text{FWHM}} = \text{const} \cdot 1.763|\beta_2(\lambda)|/\Delta\beta_1(\lambda)$, with $\Delta\beta_1$ the mean group velocity difference between the modes forming the soliton. By using the SIF dispersion parameters and the mean walk-off length for the three modes involved, and the adjustment constant const = 1.25, one predicts an initial soliton pulsewidth of 50 fs at 1450 nm, and of 103 fs at the fiber output (where the soliton wavelength moves to 1620 nm). These values agree well with both the pulsewidth obtained from simulations, and with experimental data, indicating that the theory of the walk-off soliton also applies to SI fibers, although limited to the first 3 modes. Once formed, walk-off solitons gradually evolve into monomodal solitons, carried by the fundamental LP_{01} mode of the SIF. Whereas the residual pump beam, which is composed by HOMs, has no axial intensity spot.

In conclusion, we have demonstrated the possibility of generating a spatially clean Stokes beam in the anomalous dispersion regime of SIFs, by combining the processes of soliton formation and SRS. Spatiotemporal solitons in SIFs involve the first low-order modes only; this is due to a greater difficulty, with respect to GIFs, in involving HOMs to form a single nonlinear pulse, before the modal dispersion causes a temporal separation of the HOMs. The residual wave, not involved by the process of soliton formation, is nearly lacking of the fundamental mode, with beam patterns typical of the second or third modal groups, depending on coupling conditions. Our experiments were extended, for comparison, to the case of a GIF, where the formation of spatiotemporal solitons involving higher-order axial modes is observed. In both SIFs and GIFs, the spatiotemporal solitons naturally evolve, in the range of tens of meters, into single-mode solitons.

Funding. European Research Council (740355); Ministero dell'Istruzione, dell'Università e della Ricerca (R18SPB8227); Ministerstwo Edukacji i Nauki (14.Y26.31.0017).

Acknowledgments. We thank Logan Wright et al. for making freely available the open-source parallel numerical mode solver for the coupled-mode nonlinear Schrödinger equations [18]. A modified version of the code was used for this work.

Disclosures. The authors declare no conflicts of interest.

Data availability. Data underlying the results presented in this paper are not publicly available at this time but may be obtained from the authors upon reasonable request.

References

1. A. Mecozzi, C. Antonelli, and M. Shtaif, "Coupled Manakov equations in multimode fibers with strongly coupled groups of modes," Opt. Express **20**(21), 23436–23441 (2012).
2. L. G. Wright, D. N. Christodoulides, and F. W. Wise, "Spatiotemporal mode-locking in multimode fiber lasers," Science **358**(6359), 94–97 (2017).
3. A. Hasegawa, "Self-confinement of multimode optical pulse in a glass fiber," Opt. Lett. **5**(10), 416–417 (1980).
4. A. B. Grudinin, E. Dianov, D. Korbkin, and M. P. A D. Khaidarov, "Nonlinear mode coupling in multimode optical fibers; excitation of femtosecond-range stimulated-Raman-scattering solitons," J. Exp. Theor. Phys. Lett **47**, 356–359 (1988).
5. W. H. Renninger and F. W. Wise, "Optical solitons in graded-index multimode fibres," Nat. Commun. **4**(1), 1719 (2013).

6. L. G. Wright, W. H. Renninger, D. N. Christodoulides, and F. W. Wise, "Spatiotemporal dynamics of multimode optical solitons," Opt. Express **23**(3), 3492–3506 (2015).
7. L. G. Wright, D. N. Christodoulides, and F. W. Wise, "Controllable spatiotemporal nonlinear effects in multimode fibres," Nat. Photonics **9**(5), 306–310 (2015).
8. M. Zitelli, F. Mangini, M. Ferraro, A. Niang, D. Kharenko, and S. Wabnitz, "High-energy soliton fission dynamics in multimode GRIN fiber," Opt. Express **28**(14), 20473–20488 (2020).
9. M. Zitelli, M. Ferraro, F. Mangini, and S. Wabnitz, "Single-mode spatiotemporal soliton attractor in multimode GRIN fibers," Photonics Res. **9**(5), 741–748 (2021).
10. M. Zitelli, F. Mangini, M. Ferraro, O. Sidelnikov, and S. Wabnitz, "Conditions for walk-off soliton generation in a multimode fiber," Commun. Phys. **4**(1), 182 (2021).
11. L. Rishøj, B. Tai, P. Kristensen, and S. Ramachandran, "Soliton self-mode conversion: revisiting Raman scattering of ultrashort pulses," Optica **6**(3), 304–308 (2019).
12. M. Zitelli, M. Ferraro, F. Mangini, and S. Wabnitz, "Managing self-phase modulation in pseudo-linear multimodal and monomodal systems," J. Lightwave Technol. **39**(7), 1953–1960 (2021).
13. D. Marcuse, "Loss analysis of single-mode fiber splices," Bell Syst. Tech. J. **56**(5), 703–718 (1977).
14. M. Karlsson, D. Anderson, and M. Desaix, "Dynamics of self-focusing and self-phase modulation in a parabolic index optical fiber," Opt. Lett. **17**(1), 22–24 (1992).
15. T. Hansson, A. Tonello, T. Mansuryan, F. Mangini, M. Zitelli, M. Ferraro, A. Niang, R. Crescenzi, S. Wabnitz, and V. Couderc, "Nonlinear beam self-imaging and self-focusing dynamics in a GRIN multimode optical fiber: theory and experiments," Opt. Express **28**(16), 24005–24021 (2020).
16. S. Raghavan and G. P. Agrawal, "Spatiotemporal solitons in inhomogeneous nonlinear media," Opt. Commun. **180**(4-6), 377–382 (2000).
17. F. Poletti and P. Horak, "Description of ultrashort pulse propagation in multimode optical fibers," J. Opt. Soc. Am. B **25**(10), 1645–1654 (2008).
18. L. G. Wright, Z. M. Ziegler, P. M. Lushnikov, Z. Zhu, M. A. Eftekhar, D. N. Christodoulides, and F. W. Wise, "Multimode nonlinear fiber optics: Massively parallel numerical solver, tutorial, and outlook," IEEE J. Sel. Top. Quantum Electron. **24**(3), 1–16 (2018).
19. R. H. Stolen, J. P. Gordon, W. J. Tomlinson, and H. A. Haus, "Raman response function of silica-core fibers," J. Opt. Soc. Am. B **6**(6), 1159–1166 (1989).
20. G. P. Agrawal, *Nonlinear Fiber Optics* (3 edition, Par. 2.3, Academic Pre, 2001).